Fluorescence-topographic NSOM directly visualizes peak-valley polarities of GM1/GM3 rafts in cell membrane fluctuations

Yong Chen, Jie Qin, and Zheng W. Chen[1]

Department of Microbiology and Immunology, Center for Primate Biomedical Research, University of Illinois College of Medicine, Chicago, Illinois

Abstract **Simultaneous fluorescence-topographic nanoscale imaging of cell-surface molecules in the context of membrane ultra-structures has not been reported. Here, near-field scanning optical microscopy (NSOM)-based direct fluorescence-topographic imaging indicated that GM3 rafts/nanodomains (190.0 ± 49.8 nm ranging 84.5–365.0 nm) were localized predominantly on the peaks of microvillus-like protrusions in the apical membrane of GM3 + Madin-Darby canine kidney cells, whereas GM1 rafts/nanodomains (159.5 ± 63.8 nm ranging 42–360 nm) were distributed mainly on the slops of protrusions or the valleys between protrusions in the plasma membranes of GM1 + MDCK cells. The data demonstrated that gangliosides polarized not only in a well-known apical-basolateral manner but also in the more microscopic peak-valley manner, implicating unique distribution of GM1 or GM3 in cell-surface fluctuations on the apical membrane of polarized cells. The peak-valley polarities of gangliosides also implicated their different functions relevant to lipid rafts, microvilli, or cellular processes.** Importantly, our study demonstrated for the first time that the NSOM-based direct fluorescence-topographic imaging is unique and powerful for elucidating nanoscale distribution of specific cell-surface molecules in membrane fluctuations.—Chen, Y., J. Qin, and Z. W. Chen. **Fluorescence-topographic NSOM directly visualizes peak-valley polarities of GM1/GM3 rafts in cell membrane fluctuations.** *J. Lipid Res.* 2008. **49: 2268–2275.**

Supplementary key words near-field scanning optical microscopy • fluorescent quantum dot • fluorescence-topographic imaging • ganglioside GM1 • ganglioside GM3 • MDCK • polarity

Morphological, chemical, and functional polarities of membrane lipids (1) are well described and are relevant to lipid raft formation and cellular signaling. While different lipid components, especially glycolipids, are distributed in the apical-basolateral manner in the plasma membranes of epithelial cells (2), the ganglioside-enriched rafts on T lymphocytes can redistribute asymmetrically in a leading-edge-uropod manner upon cell activation (3). Despite identification of apical-basolateral and leading-edge-uropod distributions of membrane lipids, little is known about nanostructures and precise topographic localization of gangliosides or lipid rafts in the context of biological membrane ultrastructures, such as microvilli or protrusions/valleys.

Widely used conventional imaging techniques have a limited capability to elucidate fluorescence-topographic distribution of cell-surface molecules at nanoscale. The traditional fluorescence instruments including confocal microscopy do not have enough optical resolution for detection of nanscale ganglioside clusters. Fluorescence resonance energy transfer measurement or single particle tracking technique is unable to reveal the nanoscale topographic localization of molecules on membrane surface. Rapidly developed atomic force microscopy fails to detect fluorescence information. The high-resolution electron microscopy (EM) is often limited by uncertain fidelity or reliability due to the complicated sample-preparing procedures and demanding imaging conditions.

Near-field scanning optical microscopy (NSOM) should be the best candidate for nanoscale imaging of topographic distribution of membrane gangliosides or lipid rafts, since NSOM can simultaneously provide topographic and fluorescence visualization of cell-surface molecules in nanoscale resolution (4, 5). In this study, the simultaneous fluorescence-topographic NSOM imaging, in combination with fluorescent quantum dot (QD) (4), was utilized to directly visualize nanoscale topographic-distributions of gangliosides or lipid rafts in the apical plasma membranes of Madin-Darby canine kidney cells (MDCK) cells.

Abbreviations: ATCC, American Type Collection; CTB, cholera toxin subunit B; DIC, differential interference contrast; EM, electron microscopy; FITC, fluorescein isothiocyanate; FWHM, full width at half maximum; MDCK, Madin-Darby canine kidney; MFI, mean fluorescence intensity; NSOM, near-field scanning optical microscopy; QD, quantum dot; ROI, region of interest.
[1] To whom correspondence should be addressed:
    e-mail: zchen@uic.edu

MATERIALS AND METHODS

Cell line, cell cultures, and reagents

Canine kidney MDCK epithelial cells [NBL-2; American Type Culture Collection (ATCC)] were cultured in the medium of ATCC-formulated Eagle's Minimum Essential Medium supplemented with 10% fetal bovine serum (FBS) in the 37°C, 5% CO_2 incubator. The medium was changed every 2–3 days. Subculturing was performed according to the protocol provided by the ATCC.

The reagents used in the study were as follows: biotin for negative control, biotinylated Cholera toxin subunit B (CTB) and fluorescein isothiocyanate (FITC)-conjugated CTB were purchased from Sigma; mouse IgM (kappa-chain) for isotype control and mouse anti-GM3 IgM mAb (GMR6) were purchased from BD Biosciences (San Jose, CA) and Seikagaku America (Falmouth, MA), respectively. Biotinylated goat anti-mouse IgM (μ chain) IgG mAb and streptavidin-conjugated QD655 were purchased from Invitrogen. All negative control experiments showed negative results (data now shown). To remove QD aggregates in commercial QD solution, the following procedures were followed to prepare QD dyes for use in each experiment, as mentioned previously (4). Briefly, the QD solution was spin down at 5,000 g for 5 min, a small amount (in the order of μl) of the supernatant was diluted in PBS, and then filtered/centrifuged through the Ultrafree-MC centrifugal filter devices (Millipore Corp., Bedford, MA) with ∼80–100 nm pores at 12,000 g for 5 min. The resultant supernatant was ready for use.

Confocal microscopy

To ensure that resultant supernatant of QD preparation was free of aggregates, three types of QD preparation were examined by confocal microscopy (6): the original QD solution without centrifugation and filtering (7); the QD supernatant that underwent PBS dilution and centrifugation at 5,000 g for 5 min (8); and the final QD supernatant ready for staining, as previously described. QD solution or supernatant was diluted into ∼100 μl PBS on 0.1% poly-L-Lysine (Sigma-Aldrich, St Louis, MO) coated coverglasses in the Lab-Tek chambered borosilicate coverglass system (Nalge Nunc International, Rochester, NY) and subjected to confocal microscopy. The final QD supernatant was also diluted in double distilled water and directly deposited on clean coverslip for NSOM imaging [NSOM data was shown in our previous paper (4)].

A schematic diagram is shown in Fig. 2A to image dynamic QD staining of GM1 or GM3 microdomains in the apical membranes of MDCK cells. Adherent MDCK cells grown on the sterile coverglass in the complete medium in the Lab-Tek chambered coverglass system were washed twice by 5% FBS in PBS buffer, fixed by 2% formaldehyde at 4°C for 30 min and then washed for 3 times with 5% FBS in PBS prior to staining. Then the cells were stained with biotinylated CTB for imaging of GM1-microdomains or anti-GM3 IgM plus buffer wash plus biotinylated anti-IgM mAb for imaging of GM3-microdomains at 4°C for 20 min, followed by 2%-formaldehyde fixation at 4°C for 30 min and washed two times with the buffer. The fixed, CTB-bound or primary Ab-bound MDCK cells in ∼200 μl PBS in the coverglass system were then placed on the sample stage of confocal microscope. Under confocal microscope, the freshly prepared QD solution in PBS was added into the chamber at the location away from the observed cells (as shown in Fig. 2A), and then immediately subjected to real-time confocal microscopy imaging of the cells. The QD particles diffused to the adherent cells and stained the ganglioside-enriched domains on cell surface in a time-dependent manner, therefore providing information for real-time dynamic imaging of GM1 or GM3 molcules.

To quantitatively analyze the dynamic processes of QD staining of ganglioside microdomains in plasma membranes of MDCK cells, four types of regions of interest (ROI) were classified: *i*) the regions exhibiting ganglioside microdomains as lipid raft (the bright fluorescence spots on cell surface); *ii*) the regions nearby ganglioside microdomains (representing nonspecific staining) as negative control (NC1); *iii*) the regions in solution outside cells as positive control (PC), since fluorescent QD were saturated in these regions by random diffusion before they stained cell-surface GM1 or GM3; and *iv*) the regions inside cells as negative control (NC2) since QD could not reach these regions. In each type, 10 regions (circled by numbers in Fig. 2) with the same area and radius (∼0.29 um²; radius = ∼300 nm) were selected for automatic quantification of fluorescence intensities with time lapse (during a ∼45-min period) by confocal microscopy software.

For the static imaging of ganglioside-enriched domains on MDCK cells, cells were prepared as previously described. Samples were incubated with biotinylated CTB or anti-GM3 IgM plus tiotinylated anti-IgM mAb, and washed for three times with 5% FBS in PBS, and then stained with freshly-prepared streptavidin-conjugated QD solution, followed by the 2% formaldehyde fixation at 4°C for 30 min and 2 washes with the buffer.

A Carl Zeiss LSM510 Meta5 laser scanning confocal microscope (Carl Zeiss, Thornwood, NY) was utilized in the present study. A beam of 405 nm from a diode laser, LP650 filter, and PMT were used for excitation of QD655, filtering, and detection of fluorescence. For the two-color imaging, another beam of 488 nm from an Ag/Kr laser and BP505-550 filter were applied for the FITC-conjugated CTB detection.

NSOM

For NSOM imaging, MDCK cells were cultured on sterile cover slips in 6-well plates. The MDCK-adherent cover slips were taken out from the plates and washed twice with 5% FBS in PBS, followed by fixation and immune staining as described above in the section of Confocal microscopy. After one wash with the buffer and two washes with double distilled water, the samples with MDCK cells adherent on the cover slips were air-dried and then subjected to NSOM imaging. The negative control experiments similar to what was described in the previous paper (4) were performed and all exhibited negative stainig (data not shown). The information for NSOM operation and imaging was also described in that paper (4).

Data processing and statistics

The confocal data was processed by Zeiss LSM-equipped software (Carl Zeiss, Thornwood, NY). The NSOM data, including the 2D and 3D images, and fluorescence or height profiles, was processed by NSOM-equipped SPMLab6.0.2 software (Veeco, Santa Barbara, CA), whereas the merging of NSOM topographic and fluorescence images was done with Adobe Photoshop CS3, as well as the schematic diagram. The EasyFit 4.0 software (MathWave Technologies, Dnipropetrovsk, Ukraine) was used for making histograms. Statistic analyses were performed using Student's *t*-test.

RESULTS AND DISCUSSION

Immune-conjugated QD fluorescence staining and real-time dynamics of GM3 and GM1 microdomains in apical plasma membranes of MDCK cells under confocal microscopy

As an initial effort to perform NSOM/QD-based fluorescence-topographic imaging of ganglioside-nanostructures,

static or real-time confocal microscopy was used to visualize QD fluorescence staining and dynamics of ganglioside microdomains in the apical plasma membranes of prefixed MDCK cells.

To ensure an appropriate QD staining of gangliosides on cell surface, the QD aggregates were removed from commercial stock QD solution through the centrifugation and filtration treatments (**Fig. 1A**). These treatments gave rise to high-fidelity QD preparation containing single individual streptavidin-conjugated QD655 particles [very small fraction contained two QD clusters (4)]. The QD preparation was then used to immunologically stain gangliosides GM1 and GM3 on prefixed MDCK cells and imaged under confocal microscope. Most MDCK cells were GM3+, and
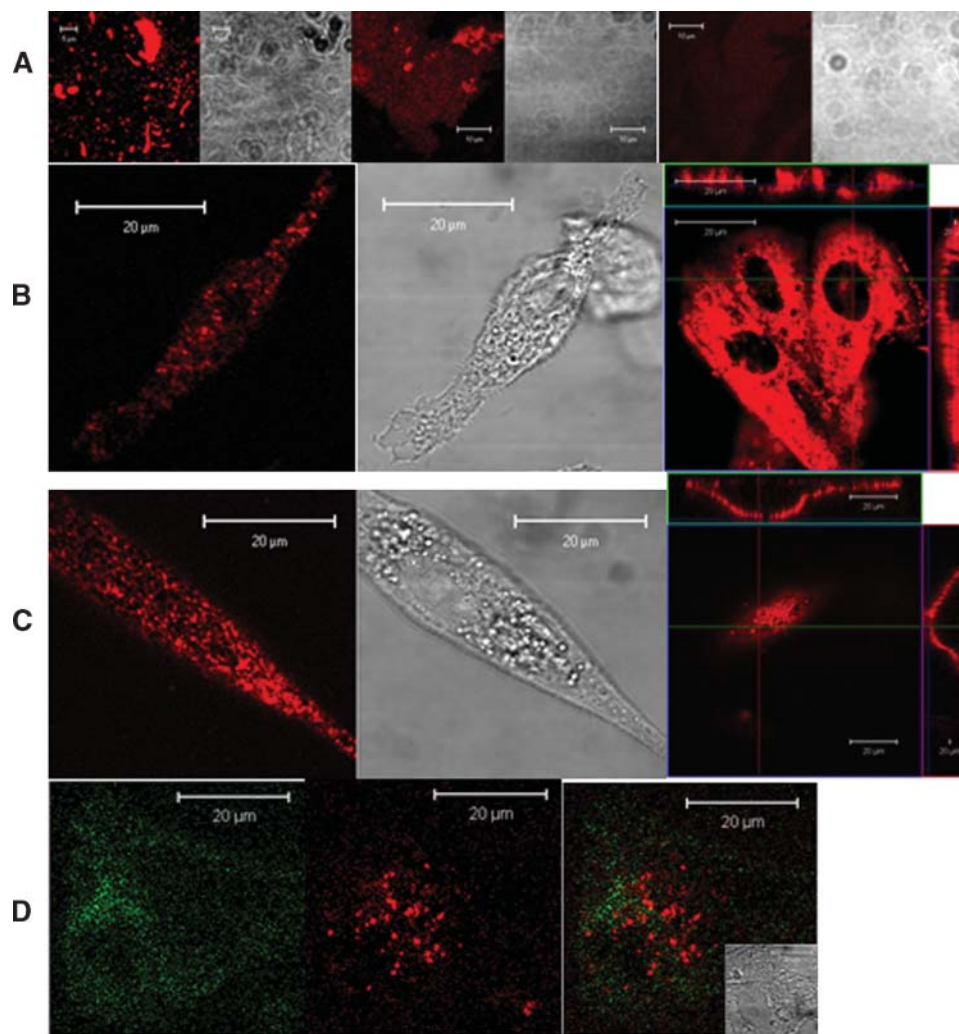

Fig. 1. Static confocal microscopic images of fluorescent quantum dot (QD) particles on substrate and QD-stained GM1 or GM3 microdomains on apical membrane of prefixed Madin-Darby canine kidney cells (MDCK) cells. A: Confocal microscopy shows that QD aggregates or large QD particles were removed for commercial QD solution by centrifugation and filtration. Treated or untreated preparations of QD solution were deposited on poly-L-lysine-coated cover slips, and imaged under static confocal microscopy. Shown are confocal images of untreated QD stock solution (left), QD supernatant after the first centrifugation at 5,000 g for 5 min (middle) and final QD supernatant treated by all the procedures: the first centrifugation, dilution in PBS, filtration ($\sim$80–100 nm-pore filter) and the second centrifugation at 12,000 g for 5 min. The near-field scanning optical microscopy (NSOM) (or transmission electron microscopy) images of the single-QD particles from the final supernatant were shown in our previous study (4). B and C show the confocal images of GM1 (B stained first with biotinylated CTB and then streptavidin-conjugated QD655) or GM3 (C stained sequentially with anti-GM3 IgM, biotinylated anti-IgM IgG, and streptavidin-conjugated QD655) microdomains on cell membrane of MDCK cells. Square images in the right panels were the top cell-membrane views of GM1 or GM3 microdomains; the rectangle images flanking the square ones were side views of membrane GM1 or GM3 as sectioned across the lines. Note that GM1 or GM3 domains were distributed most on apical membrane (square images) and some on basolateral membrane (rectangle images). D shows two-color confocal images of GM1 [green; stained with CTB- fluorescein isothiocyanate (FITC)] and GM3 (red; stained as described in C) microdomains on GM1 + GM3 + MDCK cells (inset: the DIC image).

some were GM1+, with a few cells being GM1+GM3+ (Fig. 1B–D). The GM3 or GM1 were stained as microdomains (>1000 nm) under confocal microscopy. GM1 or GM3 microdomains were mainly distributed on the apical plasma membrane as visualized on the upper surface of the cells (Fig. 1B, C, right images). Images from side views of cell sections showed that these microdomains could also be distributed in the basolateral membrane to some extent, indicating an apical-basolateral membrane distribution of these microdomains (Figs. 1B, C, right flanking rectangle
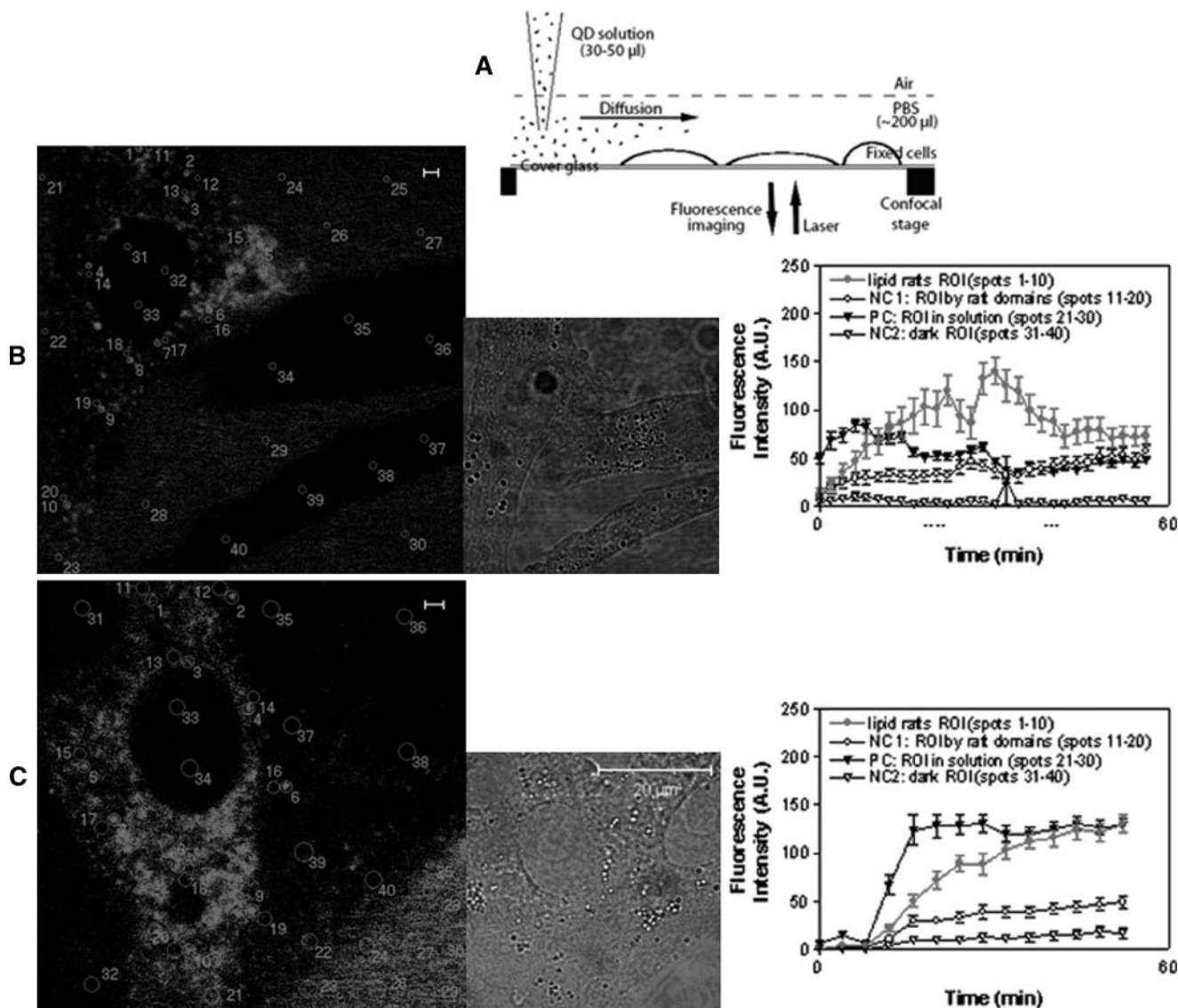

Fig. 2. Real-time confocal microscopic imaging of dynamic QD staining of GM1 or GM3 microdomains in the apical plasma membrane of MDCK cells. A: Schematic diagram for adding QD solution to MDCK cells for staining under confocal microscope. B and C were confocal images showing formation and dynamics of QD-stained GM1 and GM3 microdomains on cell surface, respectively. Left panels: snapshots of the dynamics displaying many regions of interest (ROIs) marked by circles/numbers, from which the mean fluorescence intensity (MFI) was measured. Middle panels: corresponding DIC images. Right panels: MFI vs. time graphs showing changes in mean MFI (mean ± SD) of randomly-chosen 10 ROIs corresponding to the circles as numbered in the images of the left panels. Four types of ROIs were measured: *i*) lipid raft ROI (circles 1–10 in the left images): GM1 or GM3 microdomains on cells; *ii*) NC1 (negative control 1; circles 11–20), ROI: the areas nearby the microdomains (but obviously not in the microdomains); *iii*) PC (positive control; circles 21–30), ROI: the QD solution areas outside cells, which gave rise to fluorescence due to the QD particles suspending in solution; *iv*) NC2 (negative control 2; circle 31–40), ROI: the areas inside cells, which were dark (no fluorescence) since QDs could not enter the prefixed cells. Note that MFI curves for GM1 or GM3 raft ROI were increased over time, indicating that accumulative QD staining of GM1 or GM3 microdomains instead of preformed QD aggregates binding to the GM1 or GM3 molcules. The MFI curves for PC ROI started early and relatively stable, which could be explained by the presence of QD particles in solution. No apparent increases in MFI were detected for the NC1 and NC2. Of note, the decrease in fluorescence intensity at the late stage as seen in the right graph of B was probably due to photobleaching and/or diffusion of QD particles from one to other areas of the investigated cell. The distance, concentration, and diffusion rate of QD solution together with other factors appeared to affect the speed at which the QD particles reached the cell surface for staining and therefore impacted on the MFI of QD solution around the cells, the increase in MFI for staining GM1 (B) or GM3 (C) microdomains, and the time of starting the increase. This appeared to explain why the increase in MFI for QD staining of GM1 microdomains in B started earlier than that of GM3 microdomains in C.

images). Two-color images showed that GM1 and GM3 did not colocalize on the GM1+GM3+ MDCK cells (Fig. 1D).

We then performed additional quality-control experiments to ensure that QD-stained ganglioside microdomains represent the true immune staining of GM1 or GM3 molecules, but not accumulated QD aggregates formed arguably during the staining procedure. We made use of the photobleach-resistance and brightness properties of QD particles and performed the real-time observations of the dynamic QD staining of GM1 and GM3 microdomains in the apical plasma membranes of MDCK cells. Under confocal microscope, the freshly prepared solution containing single individual streptavidin-conjugated QD was added into the cell suspension, and immediately imaged by real-time confocal microscopy for ~45 min (**Fig. 2A**, the schematic diagram and the Methods section). It was evident that the fluorescent dots of ganglioside microdomains on the cell surface became larger and brighter under real-
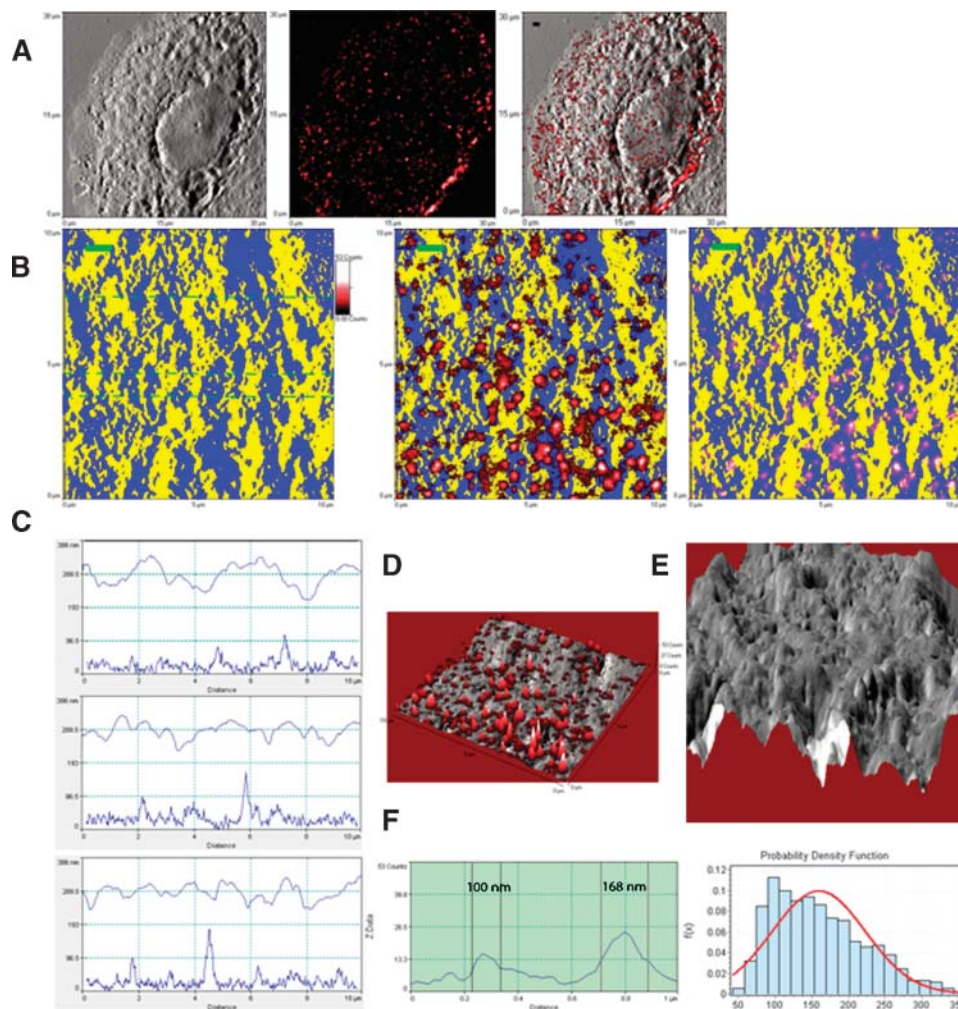

Fig. 3. Direct in situ fluorescence-topographic NSOM imaging and quantification of GM1 rafts localized predominantly in membrane valleys. A: NSOM topographic (left), fluorescence (middle), and merged (right) images of a representative GM1+ MDCK cell. B: Higher-magnification topographic (left) and fluorescence-topographic merged (middle and right) two-dimensional (2D) images of an area on the cell in Fig. 3A. The topographic information was pseudo-colored in yellow for the peak of membrane protrusions, and in blue for the planar membrane or the valley between membrane protrusions. In the middle fluorescence-topographic image, the fluorescence information (in red) was above but not merged with the topographic information (in yellow/blue), highlighting all GM1 rafts in red. In the right fluorescence-topographic image, the topographic and fluorescence information were merged, highlighting the valley-localizing GM1 rafts in pink. Scale bar = 1 μm. Note that GM1 rafts were mainly localized in planar or valley membrane. C: The height (upper curves) and corresponding fluorescence (lower curves) profiles of the cross-sections extracted from the left panel of Fig. 3B (dashed lines). Note that GM1 fluorescence corresponded to the low height areas (planar or valley membrane). D: The NSOM topographic (gray)-fluorescence (red) merged three-dimensional (3D) image of Fig. 3B shows GM1 rafts were localized in planar or valley membrane. E: The topographic 3D image of the first panel of Fig. 3B. F: left panel: the fluorescence profile extracted from a cross-section through two GM1 rafts in the middle image of Fig. 3B, with diameters (FWHM) of these nanodomains being ~100 nm and ~168 nm, respectively. Right panel: the histogram for the diameters of GM1 rafts (159.5 ± 63.8 nm; ~42 nm–360 nm). Shown is the representative of three GM1+ MDCK cells from three independent experiments.

time confocal microscopy (data not shown). Quantification analysis showed that the fluorescence intensity for the fluorescent dots of GM1 or GM3 microdomains (red curves in the right graphs of Fig. 2) was progressively enhanced with time lapse, whereas little or no increase was seen for negative control 1 (unstained areas with similar spots nearby GM1 or GM3 microdomains, representing possible non-specific staining) and negative control 2 (unstained areas inside cells where QD were unreachable). These results provided direct evidence that the fluorescent dots of GM1 or GM3 microdomains were not caused by the preformed QD aggregates during immune staining procedures.

The in situ NSOM fluorescence imaging indicated that fluorescent dots of GM3 nanodomains/rafts had a larger mean diameter (FWHM) than those of GM1 rafts

We then sought to perform in situ NSOM/QD-based nanosale fluorescence imaging of ganglioside nanodomains.

The NSOM fluorescence images (middle panels of **Figs. 3B and 4B**, and Figs. 3D and 4D) and the fluorescence profiles of the cross-sections (left panels of Figs. 3F and 4F) revealed that while GM3 and GM1 molcules were stained as fluorescence nanodomains, GM3 nanodomains looked larger and brighter than GM1 nanodomains on cell membrane. Quantification measurement showed that the mean fluorescent dots of GM3 nanodomains were 190.0 ± 49.8 nm, ranging 84.5–365.0 nm (Fig. 4F), whereas those of GM1 nanodomains were 159.5 ± 63.8 nm, ranging 42–360 nm (Fig. 3F). Both GM3 and GM1 nanodomains were comparable to the size range (10–200 nm) of ganglioside-enriched lipid raft (or membrane raft), as recently defined in the Keystone Symposium (9). The differing sizes of GM1 and GM3 may be explained by sugar components. It has been reported that increased sugar units of ganglioside can cause an increase in the lipid-water interface area that makes the ganglioside aggregates smaller (10). More sugar units in
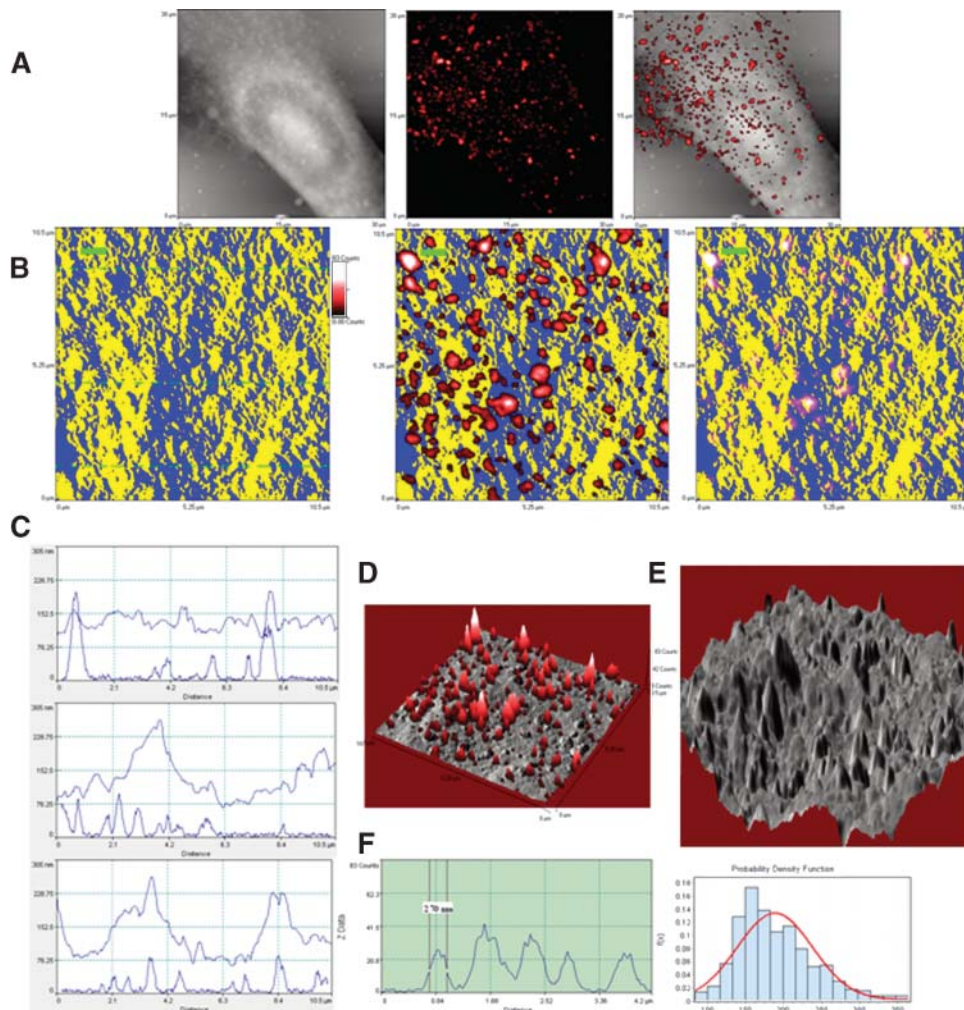

Fig. 4. Direct in situ fluorescence-topographic NSOM imaging and quantification of GM3 rafts predominantly localized in membrane peaks. The legends are the same as described in Fig. 3 except GM3 replacement for GM1. Note that in contrast to GM1, GM3 were predominantly localized in the membrane peaks as seen in B–E. In the left panel of F, one of the five GM3 rafts has a diameter of ~270 nm. In the histogram for the diameters of GM3 rafts (right panel of F), the mean diameter is 190.0 ± 49.8 nm (~84 nm–365 nm). Shown is the representative of three GM3 + MDCK cells from three independent experiments.

GM1 than in GM3 monomer may be one of the reasons why fluorescent GM1 nanodomains/rafts were smaller than fluorescent GM3 nanodomains/rafts. More abundance of GM3 molecules on MDCK cells may also be a reason for making them larger.

Direct fluorescence-topographic NSOM imaging revealed the peak-valley polarities of GM1 and GM3 rafts in cell-membrane fluctuations

Next, the exact microscopic localizations of the ganglioside nanodomains/rafts in the cell membrane ultrastructures were directly imaged by fluorescence-topographic NSOM. Under NSOM, the membrane surface of MDCK cells displayed many protrusions with various sizes as shown in the height profiles of cross-sections (Figs. 3C and 4C) or 3D NSOM topographic images (Figs. 3E and 4E). The NSOM topographic protrusions are similar in shape to previously defined microvilli, we described them as microvillus-like protrusions, but keep in mind that they are two different concepts. Since the NSOM topographic and fluorescence images were simultaneously obtained, the exact microscopic localization of the ganglioside rafts in the membrane fluctuations could be detected in the merged fluorescence-topographic images. The merged fluorescence-topographic 2D images (right panels of Figs. 3B and 4B) showed that a majority of GM1 rafts were localized in the slop of the microvillus-like protrusions of plasma membranes or on the valleys (Fig. 3B, the right panel showing GM1 rafts in pink derived from blue-red overlap). In contrast, almost all GM3 rafts were distributed on the peaks of the microvillus-like protrusions (Fig. 4B, right panel). The different distribution patterns of GM1 and GM3 rafts were also evident when topographic surface heights (upper curves) were matched for fluorescence spikes of rafts (lower curves) as scanned across sections (Figs. 3C and 4C).

The coexistence of two or more different lipid phases and the phase separation in the apical plasma membrane of epithelial cells have been reported (11). However, the phase separation was observed in the horizontal not perpendicular direction at the apical membrane plane. The colocalization of GM1 with prominin-1, a presumed microvillar marker, under confocal microscope has been taken as indirect evidence that GM1, but not GM3, may be localized in microvilli (12). However, one may argue that low-resolution confocal microscopy cannot accurately determine the real space relationship or location of two molecules unless the molecules are separated a lot from each other. Precise colocalization of two molecules might require nanoscale imaging, which is usually challenging to confocal microscopy. Virtually, the direct fluorescence-topographic nanoscal NSOM imaging demonstrates that GM3, but not GM1, are localized in microvillus-like protrusions.

Our finding that GM3, but not GM1, are localized in microvillus-like protrusions appears to be supported by other relevant studies. It has been reported that some molecules such as epidermal growth factor, human insulin receptor, glucagon receptor, and certain adhesion molecules or ion channels have a preferential initial localization in microvillus-like protrusions (6, 8, 13, 14).

The activities of these receptors or molecules can be inhibited by GM3 gangliosides through direct interaction with the receptors localized in microvillus (7, 15, 16), suggesting GM3 localizes on the microvillus-like protrusions. On the other hand, the microvillus-like protrusions are highly enriched in actin-binding proteins (13, 17), which probably provide driving forces for the polarization of molecules in local membranes.

The direct fluorescence-topographic imaging of asymmetric distribution of gangliosides implicates that gangliosides polarize not only in the apical-basolateral manner but also in a manner of a more microscopic peak-valley distribution of GM3 and GM1 on cell-membrane fluctuations in the apical membranes of polarized cells. The feature may be related to function of microvilli and various cellular processes. GM1 and GM3 membrane rafts (1, 18, 19) may have distinct function, since they are localized differently in the peak-valley manner in the apical membrane fluctuations.

Importantly, this study demonstrated for the first time that NSOM/QD-based direct fluorescence-topographic imaging is a unique, powerful tool for elucidating nanoscale topographic distribution of specific cell-surface molecules in the context of specialized membrane ultrastructures. Moreover, the fluorescence-topographic and simplicity natures of NSOM appear to be advantageous over complicated operation of conventional EM.

REFERENCES

1. Edidin, M. 2003. The state of lipid rafts: from model membranes to cells. *Annu. Rev. Biophys. Biomol. Struct.* **32:** 257–283.
2. Kawai, K., M. Fujita, and M. Nakao. 1974. Lipid components of two different regions of an intestinal epithelial cell membrane of mouse. *Biochim. Biophys. Acta.* **369:** 222–233.
3. Gomez-Mouton, C., J. L. Abad, E. Mira, R. A. Lacalle, E. Gallardo, S. Jimenez-Baranda, I. Illa, A. Bernad, S. Manes, and C. Martinez-A. 2001. Segregation of leading-edge and uropod components into specific lipid rafts during T cell polarization. *Proc. Natl. Acad. Sci. USA.* **98:** 9642–9647.
4. Chen, Y., L. Shao, Z. Ali, J. Cai, and Z. W. Chen. 2008. NSOM/QD-based nanoscale immunofluorescence imaging of antigen-specific T-cell receptor responses during an in vivo clonal Vγ2Vδ2 T-cell expansion. *Blood.* **111:** 4220–4232.
5. Enderle, T., T. Ha, D. F. Ogletree, D. S. Chemla, C. Magowan, and S. Weiss. 1997. Membrane specific mapping and colocalization of malarial and host skeletal proteins in the Plasmodium falciparum infected erythrocyte by dual-color near-field scanning optical microscopy. *Proc. Natl. Acad. Sci. USA.* **94:** 520–525.
6. Abitorabi, M. A., R. K. Pachynski, R. E. Ferrando, M. Tidswell, and D. J. Erle. 1997. Presentation of integrins on leukocyte microvilli: a role for the extracellular domain in determining membrane localization. *J. Cell Biol.* **139:** 563–571.
7. Allende, M. L., and R. L. Proia. 2002. Lubricating cell signaling pathways with gangliosides. *Curr. Opin. Struct. Biol.* **12:** 587–592.
8. Berlin, C., R. F. Bargatze, J. J. Campbell, U. H. Vonandrian, M. C. Szabo, S. R. Hasslen, R. D. Nelson, E. L. Berg, S. L. Erlandsen, and

E. C. Butcher. 1995. Alpha-4 integrins mediate lymphocyte attachment and rolling under physiological flow. *Cell.* **80:** 413–422.

9. Pike, L. J. 2006. Rafts defined: a report on the Keystone Symposium on lipid rafts and cell function. *J. Lipid Res.* **47:** 1597–1598.

10. Sonnino, S., A. Prinetti, L. Mauri, V. Chigorno, and G. Tettamanti. 2006. Dynamic and structural properties of sphingolipids as driving forces for the formation of membrane domains. *Chem. Rev.* **106:** 2111–2125.

11. Meder, D., M. J. Moreno, P. Verkade, W. L. C. Vaz, and K. Simons. 2006. Phase coexistence and connectivity in the apical membrane of polarized epithelial cells. *Proc. Natl. Acad. Sci. USA.* **103:** 329–334.

12. Janich, P., and D. Corbeil. 2007. GM(1) and GM(3) gangliosides highlight distinct lipid microdomains within the apical domain of epithelial cells. *FEBS Lett.* **581:** 1783–1787.

13. Lange, K. 2002. Role of microvillar cell surfaces in the regulation of glucose uptake and organization of energy metabolism. *Am. J. Physiol. Cell Physiol.* **282:** C1–C26.

14. Shackleton, S., I. Hamer, M. Foti, N. Zumwald, C. Maeder, and J. L. Carpentier. 2002. Role of two dileucine-like motifs in insulin receptor anchoring to microvilli. *J. Biol. Chem.* **277:** 43631–43637.

15. Miljan, E. A., E. J. Meuillet, B. Mania-Farnell, D. George, H. Yamamoto, H. G. Simon, and E. G. Bremer. 2002. Interaction of the extracellular domain of the epidermal growth factor receptor with gangliosides. *J. Biol. Chem.* **277:** 10108–10113.

16. Tagami, S., J. Inokuchi, K. Kabayama, H. Yoshimura, F. Kitamura, S. Uemura, C. Ogawa, A. Ishii, M. Saito, Y. Ohtsuka, et al. 2002. Ganglioside GM3 participates in the pathological conditions of insulin resistance. *J. Biol. Chem.* **277:** 3085–3092.

17. Hartwig, J. H., D. Brown, D. A. Ausiello, T. P. Stossel, and L. Orci. 1990. Polarization of Gelsolin and actin binding-protein in kidney epithelial-cells. *J. Histochem. Cytochem.* **38:** 1145–1153.

18. Hancock, J. F. 2006. Lipid rafts: contentious only from simplistic standpoints. *Nat. Rev. Mol. Cell Biol.* **7:** 456–462.

19. Zeyda, M., and T. M. Stulnig. 2006. Lipid Rafts & Co.: an integrated model of membrane organization in T cell activation. *Prog. Lipid Res.* **45:** 187–202.